Power Control of Grid-Connected Photovoltaic Systems

Roberto Zanasi
DII-Information Engineering Department
University of Modena and Reggio Emilia,
Via Vignolese 905, 41100 Modena, Italy
Email: roberto.zanasi@unimore.it

Stefania Cuoghi
DII-Information Engineering Department
University of Modena and Reggio Emilia,
Via Vignolese 905, 41100 Modena, Italy
Email: stefania.cuoghi@unimore.it

***Abstract*—In this paper the Power Oriented Graph technique is used for modeling a grid-connected single-phase 3kW DC/AC power converter for solar energy conversion system. A DC/DC stage, controlled by a maximum power point tracking (MPPT) technique, is used to boost the time-varying input voltage provided by photovoltaic panels. A buck DC/AC stage, including a PWM inverter, is implemented to transfer the active power to the grid. A new control scheme for the DC/AC stage is proposed.**

I. Introduction

Solar energy is currently considered to be one of the most useful natural energy sources because it is a pollution-free source of abundant power. Over the last few years, the interest in photovoltaic (PV) applications has grown exponentially. Economic evaluations show that PV technology is still too costly compared to other energetic technologies [1]. However the PV cost reduction is improving rapidly and PV systems require a very long time with almost no maintenance cost. These usually unevaluated aspects should motivate governments to deploy more PV systems [2]. Innovative inverter topologies have been suggested in the literature to provide many benefits and cost reduction. Despite modest production volumes, inverters have evolved significantly since the 1980s through manufacturer innovations and technology improvements. In 1980s inverters were bulky, heavy, difficult to install, unreliable, and their efficiency was in the $85-90\%$ range. The early 1990s saw the first large-scale series production of PV inverters (SMA PV-WR). In 1995 the first PV string inverter was produced (SMA SB 700), allowing connection of modules in series, modular systems, higher system efficiency, and reliability. Late 1990s saw basic data-acquisition system and *plug-and-play* installation. Transformerless and high frequency (HF) designs reached efficiencies above 95%. In the past $5-10$ years, inverters have evolved significantly. Reliability, ease of installation, user friendliness, efficiency, size and weight have all improved significantly. In this scenario modeling tools would be helpful to manufacturers in order to study and simulate new inverter topologies.

In this article we present an accurate model of a PV inverter architecture recently proposed in [4]. The model has been obtained using the Power Oriented Graph (POG) technique [5]. The analyzed and simulated system is based on a single-phase 3kW DC/AC power converter, implementing an active-bridge DC/DC converter and a full-bridge DC/AC. This structure performs high efficiency and the proposed digital control allows to reduce the production costs. The paper is organized as follows. In section II the system structure is presented. In section III and IV the DC/DC and DC/AC converters are analyzed and modeled. Simulations of the DC/AC converter and conclusions end the paper.

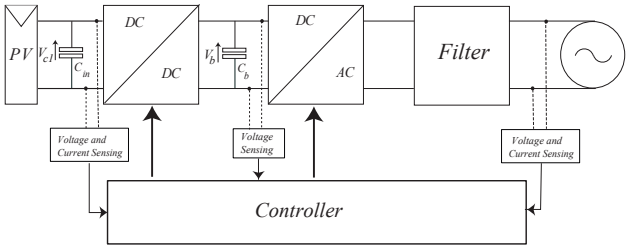

Fig. 1. Grid-connected photovoltaic system: blocks scheme.

II. System structure

Let us consider the blocks scheme of the grid-connected PV system proposed in [4] and shown in Fig. 1. The hardware section includes an active-bridge DC/DC converter which is designed to boost the input voltage from a minimum input of 150 V to a DC value regulated at 450 V. Then a single-phase buck 3kW DC/AC converter is employed to step down and to modulate the output voltage according to the grid voltage (230 Vrms $\pm 10\%$ and $49.7-50.3$ Hz). Finally the filter is designed to reduce high-order harmonics introduced by the PWM modulation of the DC/AC converter. The control of the system is obtained by a microprocessor. The phase-shift control between the input bridge legs and the output bridge legs of the DC/DC converter is determined by a Maximum Power Point Tracking (MPPT) algorithm, in order to extract the maximum possible power from the PV panels in all the irradiation conditions. The control of the DC/AC converter is designed to supply current into the utility line by regulating the bus voltage V_b to 450V. The control of the power flow to the grid, according to the European standards (EN 61727), is based on the control of active and reactive power. The required synchronization between the grid voltage and the

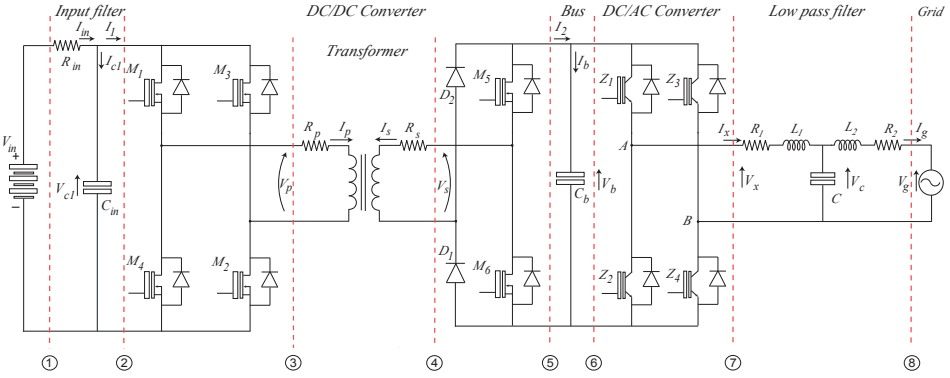

Fig. 3. Complete hardware structure of the PV system connected to the grid.

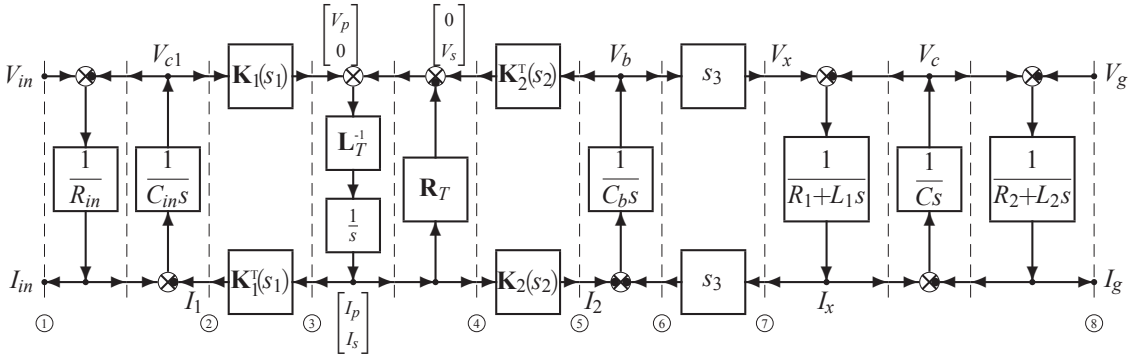

Fig. 4. Corresponding POG model of the PV system connected to the grid.

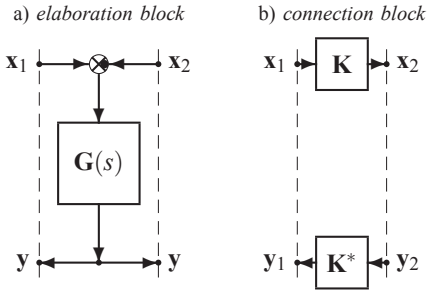

Fig. 2. POG: a) *elaboration block*; b) *connection block*.

voltage generated by the converter is done by using a Phase Locked Loop (PLL) algorithm which detects the phase angle of utility voltage. More details of the system operation are given in Sec. III and IV.

The Power-Oriented Graphs, see [5]-[7], is a graphical modeling technique suitable for modeling physical systems. The POG are normal block diagrams combined with a particular modular structure essentially based on the use of the two blocks shown in Fig. 2: the *elaboration block* stores and/or dissipates energy (i.e. springs, masses, dampers, capacities, inductances, resistances, etc.); the *connection block* redistributes the power within the system without storing or dissipating energy (i.e. any type of gear reduction, transformers, etc.). The main feature of the Power-Oriented Graphs is to keep a direct correspondence between the dashed sections of the graphs and real power sections of the modeled systems: the scalar product $\mathbf{x}^{\mathrm{T}}\mathbf{y}$ of the two *power vectors* $\mathbf{x}$ and $\mathbf{y}$ involved in each dashed line of a power-oriented graph, see Fig. 2, has the physical meaning of *the power flowing through that particular section*. Note, for example, that the dashed lines ①-⑧ in Fig. 4 are in direct correspondence with the physical power sections ①-⑧ of Fig. 3: ①-② is the input filter, ②-⑤ is the DC/DC converter which includes the input bridge, the high frequency (HF) transformer and the output bridge, ⑤-⑦ includes the bus capacitor C_b and the DC/AC converter and ⑦-⑧ is LCL filter. It is easy to see that the state space equations of the POG model of Fig. 4 can be expressed in the form $\mathbf{L}\dot{\mathbf{x}} = -\mathbf{A}\mathbf{x} + \mathbf{B}\mathbf{u}$ where:

$$\mathbf{L} = \begin{bmatrix} C_{in} & 0 & 0 & 0 & 0 & 0 \\ 0 & \mathbf{L}_T & 0 & 0 & 0 & 0 \\ 0 & 0 & C_b & 0 & 0 & 0 \\ 0 & 0 & 0 & L & 0 & 0 \\ 0 & 0 & 0 & 0 & C & 0 \\ 0 & 0 & 0 & 0 & 0 & L \end{bmatrix}, \quad \mathbf{x} = \begin{bmatrix} V_{c1} \\ \mathbf{I}_{ps} \\ V_b \\ I_x \\ V_c \\ I_g \end{bmatrix}, \quad \mathbf{I}_{ps} = \begin{bmatrix} I_P \\ I_s \end{bmatrix},$$

$$\mathbf{A} = \begin{bmatrix} \frac{1}{R_{in}} & \mathbf{K}_1^{\mathrm{T}} & 0 & 0 & 0 & 0 \\ -\mathbf{K}_1 & \mathbf{R}_T & -\mathbf{K}_2^{\mathrm{T}} & 0 & 0 & 0 \\ 0 & \mathbf{K}_2 & 0 & s_3 & 0 & 0 \\ 0 & 0 & -s_3 & R_1 & 1 & 0 \\ 0 & 0 & 0 & -1 & 0 & 1 \\ 0 & 0 & 0 & 0 & -1 & R_2 \end{bmatrix}, \quad \mathbf{B} = \begin{bmatrix} \frac{1}{R_{in}} & 0 \\ 0 & 0 \\ 0 & 0 \\ 0 & 0 \\ 0 & 0 \\ 0 & -1 \end{bmatrix},$$

$$\mathbf{u} = \begin{bmatrix} V_{in} \\ V_g \end{bmatrix}, \quad \mathbf{L}_T = \begin{bmatrix} L_p & M \\ M & L_s \end{bmatrix}, \quad \mathbf{R}_T = \begin{bmatrix} R_p & 0 \\ 0 & R_s \end{bmatrix}, \quad \mathbf{K}_1(s_1) = [s_1 \ 0]^{\mathrm{T}}, \quad \mathbf{K}_2(s_2) = [0 \ s_2].$$

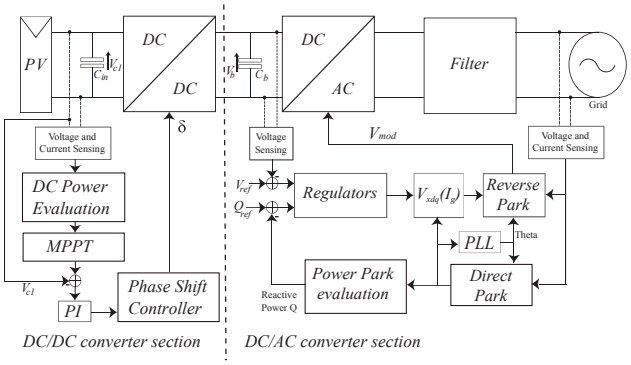

Fig. 5. Power Management Control (PMC) scheme

III. DC/DC CONVERTER SECTION

Let us now consider the POG model of the single-phase phase-shifted DC/DC converter shown in Fig. 4 between sections ②-⑤: it is composed by an input full bridge (FB) connected to an active half bridge (HB) through an HF transformer. This structure provides galvanic isolation between the PV array and the utility line, protecting the system against electric shock and improving its safety. The DC/DC converter is controlled using the zero-voltage-switching (ZVS) PWM technique [8] and operates in a soft-switched manner [9]. The operating principle of the converter is described in [4] with the variant of using an active HB instead of active FB. The time behaviors of the main variables of the DC/DC converter are shown in Fig. 6. Variable $M_i(t)$ denotes the control input of the i-th MOS: when $M_i = 1$ the MOS is ON, when $M_i = 0$ the MOS is OFF. The DC/DC converter is controlled by regulating the phase-shift δ between signal $M_5(t) = \overline{M}_6(t)$ of the active bridge (dashed red line) and signal $M_1(t) = M_2(t)$ of the input bridge (blue line). Note that the signals $M_3(t) = M_4(t)$ are not represented in Fig. 6 because they are equal to signal $\overline{M}_1$ except during dead time when all MOS of input bridge are OFF. The basic structure of the control algorithm of the DC/DC converter is shown in Fig. 5: it is based on the Maximum Power Point Tracking (MPPT) algorithm and it implements an optimized version of the *perturb and observe method* described in [4] and [10]-[12]. This method regulates the phase-shift δ and it is based on the sensing of current and voltage of PV array and on the estimation of DC output power: the DC current I_2 is chosen to maximize the power operating point of the PV system.

In Fig. 6, the signals $V_p(t)$, $I_p(t)$ (blue lines) and $V_s(t)$, $I_s(t)$ (dashed red lines) represent, respectively, the primary and secondary voltage and current of the transformer. The dynamic model of the input bridge is described in Fig. 4 by the connection block ②-③ characterized by matrix $\mathbf{K}_1(s_1)$. The control signal $s_1(t)$ in time-domain is obtained as follows, neglecting the dissipative losses of the MOS (see blue line in Fig. 6-*b*):

$$s_1(t) = \frac{V_p(t)}{V_{c1}(t)} = \frac{I_1(t)}{I_p(t)} = 2\left(M_1(t) \oplus \overline{M}_3(t)\mathrm{sgn}\bar{I}_p(t) - 0.5\right),$$

where $V_{c1}(t)$ and $I_1(t)$ are respectively the input voltage and current. The dynamic model of the output active bridge is described in Fig. 4 by the connection block ④-⑤ characterized by matrix $\mathbf{K}_2(s_2)$. The control signal $s_2(t)$ can be expressed as follows (see dashed red line in Fig. 6-*b*):

$$s_2(t) = \frac{V_s(t)}{V_b(t)} = \frac{I_2(t)}{I_s(t)} = \left(M_5(t)\bar{I}_s(t) - \overline{M}_5(t)I_s(t)\right),$$

where $V_b(t)$ and $I_2(t)$ are the output bus voltage and current. In Fig. 4, the dynamic model of the transformer is described in section ③-④ by using the matrices $\mathbf{L}_T$ e $\mathbf{R}_T$: L_p, L_s and M are the self and mutual inductances of the transformer, R_p and R_s are the corresponding transformer resistances. The power P_{av} transferred to the output in half switching period can be expressed as follows:

$$P_{av} = \frac{V_{c1}^2 d\pi}{2\omega L(2+d)^2}\left[1 + d - 2d^2 + \left(\frac{\delta}{\pi}\right)4(d^2+d+1) - \left(\frac{\delta}{\pi}\right)^2 2(d^2+2d+2)\right], \quad (1)$$

where ω is the switching frequency, L is the primary-referred leakage inductance, n is the transformer turn ratio, $d = \frac{V_b}{nV_{c1}}$ and δ is the phase shift between the input and the output bridges. Relation (1) has been obtained using the a method similar to the one described in [4] for the active full bridge.

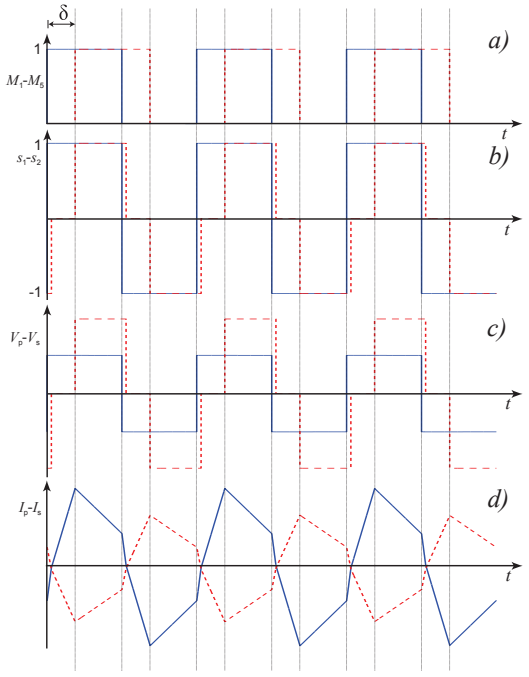

Fig. 6. Time behaviors of the main variables of the DC/DC converter.

IV. DC/AC CONVERTER SECTION

Let us now consider the POG model shown in Fig. 4 between sections ⑥ and ⑧: it is composed by a IGBT full-bridge DC/AC converter PWM-controlled and a LCL low pass filter. The filter is used to reduce the high-frequency harmonics

introduced by the PWM modulation on output voltage. The considered control scheme is shown in Fig. 5: the controller is designed to transfer to the grid, according to the European standard, the DC power provided by the DC/DC converter section. The DC/AC converter is modeled in Fig. 4 by the connection block situated between sections ⑥ and ⑦. The DC/AC converter is controlled by single-phase unipolar PWM modulation. The main advantage of this technique is that no spectral bins appear at the odd multiples of the switching frequency, and no multiples of the switching frequency are present. This essentially doubles the switching frequency, thus allowing the specifications of the LCL filter to be relaxed. The voltages of points A and B in Fig. 3 are separately regulated comparing the PWM triangular carrier $V_t(t)$ with the modulation voltage $V_{mod}(t)$ normalized with respect to the bus voltage $V_b(t)$. The control signal $s_3(t)$ can be expressed as follows:

$$s_3(t) = \frac{\text{sgn}\left(V_t(t) + \frac{V_{mod}(t)}{V_b(t)}\right) - \text{sgn}\left(V_t(t) - \frac{V_{mod}(t)}{V_b(t)}\right)}{2}, \quad (2)$$

thus the modulated voltage $V_x(t) = s_3(t)V_b(t)$ switches between the three levels $\{+V_b, -V_b, 0\}$.

The structure of the LCL filter is shown in Fig. 4, sections ⑦-⑧. The filter has been designed to reduce the high-order harmonics on the grid side according to the method described in [13] and [4]. In the Laplace's domain, the transfer functions $G_x(s) = I_g(s)/V_x(s)$ and $G_g(s) = I_g(s)/V_g(s)$ have the following structure:

$$G_x(s) = \frac{G_1 G_2 G_3}{1 + G_1 G_2 + G_2 G_3}, \quad G_g(s) = \frac{-G_1 G_2 G_3 + G_3}{1 + G_1 G_2 + G_2 G_3}, \quad (3)$$

where:

$$G_1 = \frac{1}{L_1 s + R_1}, \qquad G_2 = \frac{1}{Cs}, \qquad G_3 = \frac{1}{L_2 s + R_2}.$$

As shown in the Bode diagram of the frequency response $G_x(j\omega)$ of Fig. 7, the LCL filter introduces a phase shift and a gain at the grid frequency ω_g. The modulation voltage $V_{mod}(t)$ has to be chosen to compensate the filter effects and to synchronize the grid current $I_g(t)$ with the grid voltage $V_g(t)$. In the space vector representation the modulation voltage can be expressed as the complex number $\overline{V}_{mod} = V_x(s)|_{s=j\omega_g}$, where $V_x(s)$ can be expressed as follows from (3):

$$V_x(s) = V_g(s)\,(1 + R_1 Cs + L_1 Cs^2) + I_g(s)\,(L_1 L_2 Cs^3 + \\ + (L_1 R_2 + L_2 R_1) Cs^2 + (R_1 R_2 C + L_1 + L_2)s + R_1 + R_2). \quad (4)$$

The grid voltage is given by sensing system while the desired grid current is given by the feedback control loop shown in Fig. 5. This control scheme is an improved version of the control algorithm described in [4]. In particular, using an indirect control, the grid current $I_g(t)$ is chosen to force the bus voltage $V_b(t)$ to be equal to a desired reference value V_{bref} in order to balance the power flowing through the system. The considered control scheme becomes very simple using the Park transformations and Akagi's pq theory [14]-[19]. Referring

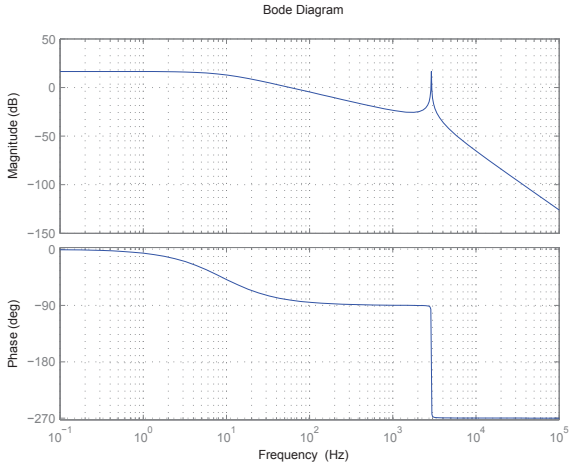

Fig. 7. Bode diagrams of the transfer function $G_x(s)$ for $C = 5\,\mu F$, $L_1 = 1.8\,mH$, $L_2 = 0.9\,mH$, $R_1 = 0.1\,\Omega$, $R_2 = 0.05\,\Omega$.

to the notation used in [19], the sinusoidal signals can be expressed using a rotating space vector, i.e.

$$u(t) = U e^{j(\omega t + \phi)}. \quad (5)$$

In stationary (x, y) reference frame, (5) can be written in the form $u(t) = u_x(t) + j u_y(t)$, where the x and y components are $u_x(t) = U\cos(\omega t + \phi)$ and $u_y(t) = U\sin(\omega t + \phi)$. The following Park transformation matrix

$$\mathbf{T}_D = \begin{bmatrix} \cos\theta & \sin\theta \\ -\sin\theta & \cos\theta \end{bmatrix}$$

converts the u_x and u_y components $\mathbf{u}_{xy} = [u_x(t)\ u_y(t)]^T$ into dq components $\mathbf{u}_{dq} = [u_d\ u_q]^T$, which are constants in steady-state in a rotating reference frame. The inverse Park transformation is: $\mathbf{u}_{x,y} = \mathbf{T}_D^T \mathbf{u}_{d,q}$. Using the Park transformation matrix $\mathbf{T}_D$, the grid voltage $V_g(t)$ and the grid current $I_g(t)$ are converted in constant variables in the dq frame: $\overline{V}_{gdq}(t) = V_{gd}(t) + jV_{gq}(t)$ and $\overline{I}_{gdq}(t) = I_{gd}(t) + jI_{gq}(t)$. The angle θ used in the transformation matrix $\mathbf{T}_D$, is obtained using a digital Phase-Locked Loop (PLL) designed in the rotating dq frame, see [4] and Fig. 9.

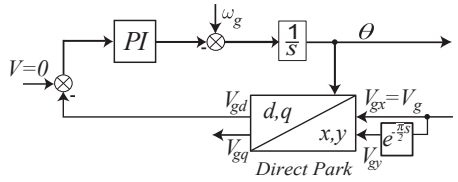

Fig. 9. Block diagram representation of PLL algorithm

The "Power Park evaluation" block shown in Fig. 5 calculates the active power P and the reactive power Q flowing towards the grid: $\overline{P}(t) = P(t) + jQ(t) = \overline{V}_{gdq}(t)\,\overline{I}_{gdq}(t)$. In the dq frame, the desired grid current can be expressed as follows: $\overline{I}_{gref}(t) = I_{dref}(t) + j\,I_{qref}(t)$. The reactive grid current $I_{dref}(t)$

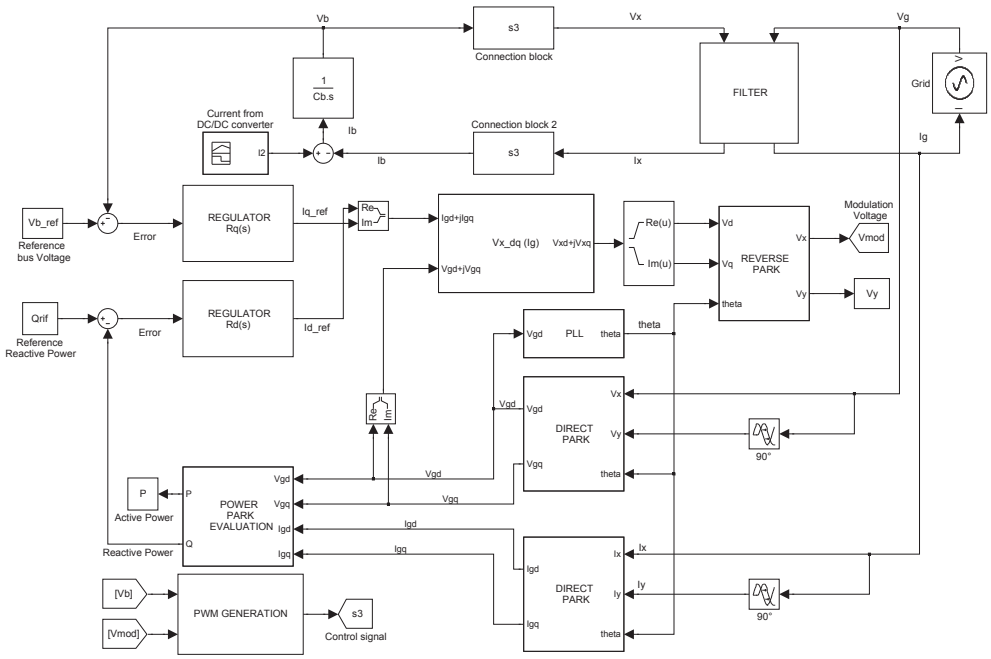

Fig. 8. Simulink scheme of DC/AC section implemented for the model validation.

is regulated by a PI compensator in order to have zero reactive power Q. The active grid current $I_{qref}(t)$ is dynamically controlled by a second PI compensator in order to maintain the bus voltage $V_b(t)$ equal to the desired value V_{bref}. Notch filters are inserted in cascate to the PI regulators in order to filter the high frequency ripple due to PWM modulation. Note that the inner double PI structure used in [4] to generate the modulation voltage in the dq frame is here substituted by block "$V_{xdq}(I_g)$" shown in Fig. 5 which is defined as follows, see relation (4):

$$\begin{aligned} V_{xdq}(t) = \quad & \bar{V}_{gqd}(t)(1-L_1C\omega_g^2+jR_1C\omega_g)+ \\ & +\bar{I}_{gref}(t)[R_1+R_2-(L_1R_2+L_2R_1)C\omega_g^2+ \\ & +j((R_1R_2C+L_1+L_2)\omega_g-L_1L_2C\omega_g^3)], \end{aligned}$$

where $V_{gdq}(t)$ is the grid voltage expressed in the dq frame. The DC/AC control voltage $V_{mod}(t)$ is finally obtained from $\bar{V}_{xdq}(t)$ using the inverse Park transformation.

V. Validation of the Model and Simulation Results

Due to the complexity of the overall system, in this paper we present only the simulation results of the DC/AC section, see the Simulink scheme in Fig. 8. The simulation results have been obtained using the following parameters: PWM carrier frequency $\omega_c = 17kHz$; grid frequency $\omega_g = 50Hz$; filter parameters: $C = 5\,\mu F$, $L_1 = 1.8\,mH$, $L_2 = 0.9\,mH$, $R_1 = 0.1\,\Omega$, $R_2 = 0.05\,\Omega$; $V_{bref} = 450$ V; the PI controller $R_q(s)$ of variable I_{qref}: $R_q(s) = 1.8 + \frac{25}{s}$; the PI controller $R_d(s)$ of variable I_{dref}: $R_d(s) = 0.001 + \frac{0.01}{s}$; the PI controller $R_L(s)$ in the PLL algorithm: $R_L(s) = 1 + \frac{30}{s}$.

The waveform of the main system signals when a step input current $I_2 = 7A$ is applied are shown in Fig. 10-12. In particular, Fig. 10 shows the dynamical behavior of grid voltage $V_g = V_{g0}\sin(\omega_g t)$ and grid current I_g. The zoom

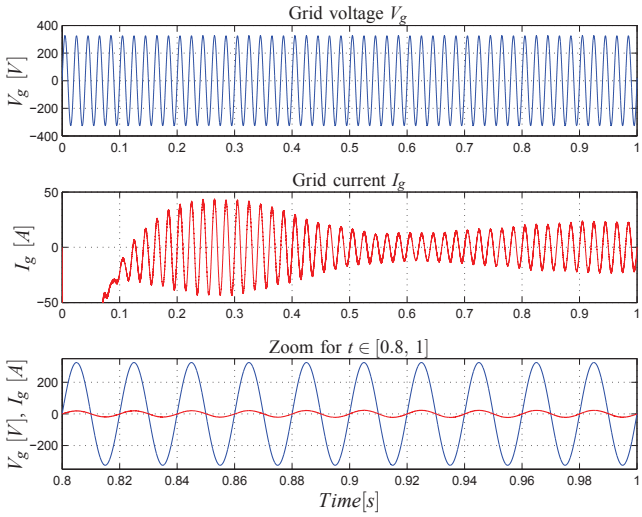

Fig. 10. Step responses of grid voltage Vg and grid current I_g for $I_2 = 7A$.

in Fig. 10 clearly shows the good synchronization between signals V_g and I_g. The Park transformed signal $\bar{V}_{gdq}$ is exactly equal to the expected value: $\bar{V}_{gdq} = -jV_{g0}$. The bus voltage V_b and the control signals I_{dref} and I_{qref} generated in the rotating frame by regulators $R_q(s)$ and $R_d(s)$ are shown in Fig. 11. The powers P_5, P_6 and P_8 flowing through different sections of the system in steady-state condition are shown in Fig. 12. In particular the blue line represents the input power $P_5 = V_bI_2$ flowing through section ⑤, while the black and red lines represent the powers flowing through sections ⑥ and ⑧ of the POG scheme of Fig. 4. The ripple present on the power signals is mainly due to the current ripple and it depends on

the *LCL* filter design [4]. The magenta and green lines shown Fig. 12 represent the active power P and the reactive power Q flowing towards the grid. In particular one can notice that the mean value of Q is equal to zero and the mean value of P is nearly equal to power P_5. The system currents I_2, I_{gd}, I_{gq}, I_{dref} and I_{qref} obtained with a I_2 sawtooth reference are shown in Fig. 13, see [4].

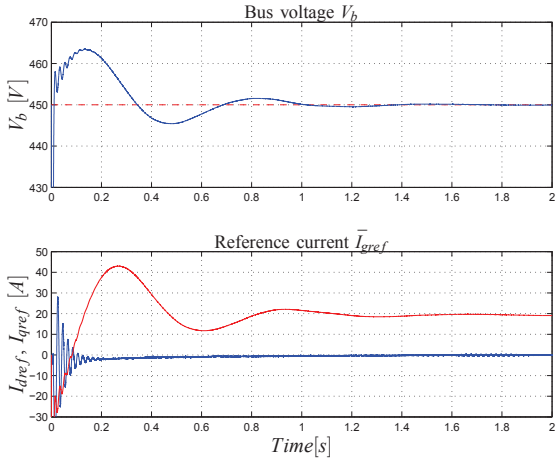

Fig. 11. Bus voltage V_b, reference active grid current I_{qref} (red) and reactive grid current I_{dref} (blue).

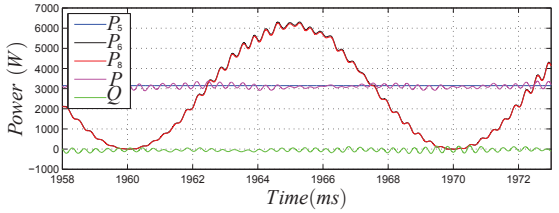

Fig. 12. Power flows P_5, P_6 and P_8 through sections 5, 6 and 8 of the POG scheme of Fig. 4. Active and reactive powers P and Q.

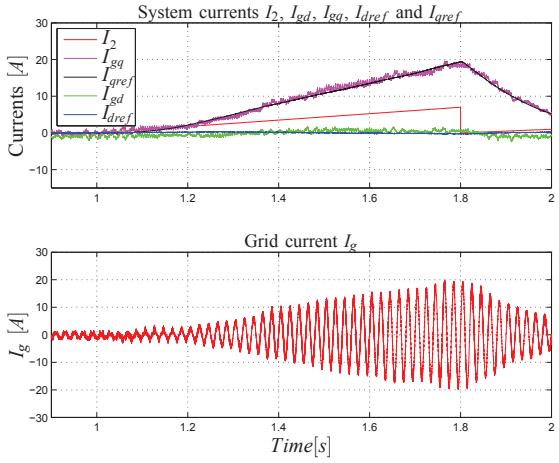

Fig. 13. Main system currents when I_2 is a sawtooth reference.

VI. Conclusion

In this paper a recent and innovative inverter for PV system grid-connected is modeled using the POG technique. The main advantages of the proposed approach are the direct correspondence between POG sections and real power sections of the modeled system and the easy implementation of the POG graphs in Matlab-Simulink environment [7]. A simplified and robust control structure has been proposed. The presented simulation results confirm the validity of the model and seems to be useful to reduce the Levelized Energy Cost for photovoltaic systems.

Acknowledgment

The authors would like to thank S. Culzoni, C. Tebaldi and M. Candeli.

References

[1] EIA, 2011, *Levelized cost of new generation resources in the Annual Energy Outlook* 2011. U.S. Energy Information Administration.

[2] K. Zweibel, *Should solar photovoltaics be deployed sooner because of long operating life at low, predictable cost?* Energy Policy, 38:7519-7530,2010.

[3] *Review of PV inverter technology cost and performance projections*. Nat. Renewable Lab. Energy, Golden, CO, NREL Report SR-620-38771, 2006.

[4] M. Cacciato, A. Casoli, R. Attanasio and F. Gennaro *Soft-switching converter with HF transformer for grid-connected photovoltaic systems*, IEEE Transactions on Industrial Electronics, 57(5):1678-86,2010.

[5] R. Zanasi, "The Power-Oriented Graphs technique: System modeling and basic properties", Vehicle Power and Propulsion Conference (VPPC), 2010 IEEE, Lille, France, 1-3 Sept. 2010

[6] R. Zanasi, G. H. Geitner, A. Bouscayrol, W. Lhomme, "Different energetic techniques for modelling traction drives", ELECTRIMACS 2008, Qubec, Canada, June 8-11 2008.

[7] R. Zanasi, "Power Oriented Modelling of Dynamical System for Simulation", IMACS Symp. on Modelling and Control, Lille, France, May 1991.

[8] Y. Jang, M. Jovanovic, Y. Chang, *A new ZVS-PWM full-bridge converter*. IEEE Trans. on Power Electron.: 18(5):1122-1129, Sept. 2003.

[9] R.W. De Doncker, D.M. Divan, M.H. Kheraluwala, *A three-phase soft-switched high-power-density DC/DC converter for high-power applications*. IEEE Trans. on Industry Applications: 27(1):63-73, Jan/Feb 1991.

[10] N. Femia, G. Petrone, G. Spagnuolo, and M. Vitelli, *Optimization of perturb and observe maximum power point tracking method*. IEEE Trans. Power Electron.: 20(4): 963973, Jul. 2005.

[11] D. Sera, R. Teodorescu, J. Hantschel, and M. Knoll, *Optimized maximum power point tracker for fast-changing environmental conditions*. IEEE Trans. Ind. Electron.: 55(7): 26262637, Jul. 2008.

[12] T. Esram and P. L. Chapman, *Comparison of photovoltaic array maximum power point tracking techniques*. IEEE Trans. Energy Convers.: 22(2):439449, Jun. 2007.

[13] M. Liserre, R. Teoderuscu, and F. Blaabjerg, *Stability of photovoltaic and wind turbine grid-connected inverters for a large set of grid impedance values*. IEEE Trans. Power Electron.: 21(1), 263272, Jan. 2006.

[14] J.M. Kwon, K.H. Nam and B.H. Kwon. *Photovoltaic power conditioning system with line connection*. IEEE Trans.Ind.Electron.: 53(4):1048-1054, Jun. 2006.

[15] R. Teodorescu and F. Blaabjerg, *Flexible control of small wind turbines with grid failure detection operating in stand-alone and grid-connected mode*. IEEE Trans. on Power Electron.: 19(5):1323-1332, Sept. 2004.

[16] A. Yazdani and R. Iravani, *Voltage-Sourced Converters in Power Systems*. IEEE Pressed 2010.

[17] K. J. strm and B. Wittenmark, *Computer-Controlled Systems Theory and Design*. 3rd ed. Englewood Cliffs, NJ: Prentice-Hall, 1984.

[18] H. Akagi, Y. Kanagawae, and A. Nabae, *Instantaneous reactive power compensator comprising switching devices without energy storage components*. IEEE Trans. Ind. Appl.:IA-20(3), 625634, May/Jun. 1984.

[19] L. G. B. Rolim, D. R. da Costa, and M. Aredes, *Analysis and software implementation of a robust synchronizing PLL circuit based on the pq theory*. IEEE Trans. Ind. Electron.: 53(6), 19191926, Dec. 2006.